Sensors and Materials, Vol. 36, No. 11 (2024) 4865–4879
MYU Tokyo

S & M 3836

Robust Sliding Mode Speed Control of Permanent Magnet Synchronous Motor with Time Delay Estimation

An-Po Lin,[1] Bo-Wun Huang,[1] Chih-Hung Hsu,[2] Po-Hsun Chen,[3] Cheng-Yi Chen,[3*] and Cheng-Fu Yang[4,5**]

[1]Institute of Mechatronic Engineering, Cheng Shiu University, Kaohsiung 833, Taiwan
[2]Department of Electrical Engineering, National Sun Yat-Sen University, Kaohsiung City 80424, Taiwan
[3]Department of Electrical Engineering, Cheng Shiu University, Kaohsiung City 833, Taiwan
[4]Department of Chemical and Materials Engineering, National University of Kaohsiung, Kaohsiung 811, Taiwan
[5]Department of Aeronautical Engineering, Chaoyang University of Technology, Taichung 413, Taiwan

(Received April 30, 2024; accepted September 2, 2024)

Keywords: sliding mode, speed control, time delay estimation, permanent magnet synchronous motor

In industrial automation systems, motors are crucial in driving mechanisms for speed or positioning control tasks. The widespread adoption of AC motors has been driven by their advantages such as low cost, solid structure, and easy maintenance. AC motors have gradually supplanted traditional DC motors with brushes and commutators and have become the predominant choice for motor and drive applications in industrial settings. In this paper, we introduce a hybrid control scheme that combines a sliding mode controller (SMC) and time delay estimation to enhance the robustness of speed control for permanent magnet synchronous motors (PMSM). Following the field-oriented principle, a flux SMC is initially designed to meet stator flux control requirements promptly. Subsequently, a speed controller is introduced, employing SMC with time delay estimation to address challenges such as torque and flux ripples, ultimately enhancing the overall robustness of the control system. Simulation results validate the effectiveness of the proposed control scheme under conditions of load disturbance and parameter uncertainties. Future work will involve implementing the proposed approach on digital signal processors to validate its performance and practicality in real-world applications.

1. Introduction

Motors are pivotal in propelling mechanical loads for constant speed or positioning tasks within industrial automation systems. The widespread adoption of AC motors, owing to their affordability, sturdy structure, and easy maintenance, has led to the gradual displacement of traditional DC motors. AC motors have become the predominant choice for motor drives in industrial applications and servo control. The permanent magnet synchronous motors (PMSM) is a specific type of AC motor, in which the rotor features a permanent magnet capable of self-excitation. This magnet interacts with the stator flux of the three-phase armature winding, facilitating rotation. In contrast to induction motors, which rely on stator magnetic flux induction

*Corresponding author: e-mail: k0464@gcloud.csu.edu.tw
**Corresponding author: e-mail: cfyang@nuk.edu.tw
https://doi.org/10.18494/SAM5106

ISSN 0914-4935
https://myukk.org/

to generate rotor currents, PMSMs simplify the process of magnetic energy conversion. This simplification results in reduced conversion losses and improved operational efficiency. In recent decades, researchers have dedicated considerable efforts to tackling challenges in AC motor drive control systems.[1–7] In high-performance PMSM servo systems, common vector control methods include field-oriented control (FOC)[1–4] and direct torque control (DTC).[5–7] FOC involves intricate decoupling calculations and is susceptible to variations in motor parameters and external load changes.[8]

DTC employs torque and stator flux hysteresis comparators to address these challenges and identify error states. Subsequently, by utilizing a switching table, the optimal voltage space vectors are directly selected to regulate torque and stator flux.[9-11] The DTC approach eliminates the need for decoupling calculations, ensuring excellent torque response. Additionally, its control architecture is simple and easily implementable. However, traditional DTC faces limitations, as it can only choose eight primary voltage vectors per control cycle. This limitation results in difficulty controlling torque and flux at low speeds, significant torque and flux ripples, nonfixed switching frequencies, and high noise levels.[12] Another control strategy is voltage frequency control. It is renowned for straightforward control system architecture, stability, ease of maintenance, and avoidance of complex mathematical model computations or considerations of relevant electrical parameters.[13,14] Despite these advantages, the speed control of PMSMs often yields undesirable speed responses in practical applications owing to low starting torque, slow response speed, and insufficient precision. Recent advancements in power electronics, microprocessor technology, and magnetic materials have facilitated the implementation of intricate control algorithms.

Consequently, by incorporating proposed vector control methods, PMSM drive systems have progressively supplanted DC motors in industrial applications. This shift has expanded their usage in diverse areas, including machine tools, industrial robots, and elevator systems. The proposed inverter modulation strategy primarily relies on the space vector modulation (SVM) technique, offering advantages such as enhanced linear modulation factors, improved DC voltage regulation rates, and reduced total harmonic distortion. Integrating SVM into the traditional DTC framework effectively mitigates torque and flux ripples. Taghizadegan *et al.*[15] integrated SVM technology with DTC and introduced a proportional-integral (PI) controller to rectify torque and stator flux errors. This approach utilizes stator voltage vectors generated by SVM to drive PMSM operation. It is aimed at ameliorating torque and flux ripple phenomena while maintaining robust transient and steady-state performance. Similarly, Zhou *et al.*[16] suggested the utilization of digital signal processors and complex programmable logic devices to estimate the magnitude and angular position of the rotor flux vector. This overall structure, incorporating SVM, ensures excellent speed dynamic performance.

However, it is worth noting that while PI controllers are more easily implemented with single-chip solutions in industrial control applications, their adaptation of controller parameters through linear control analysis and design can maintain speed dynamic performance.[17] Nevertheless, PI controllers are susceptible to decreased speed control accuracy and adverse dynamic responses owing to factors such as variations in system parameters, disturbances from external loads, and interference from noise. Utilizing a sliding mode controller (SMC) offers a

means of compensating system uncertainties arising from parameter variations or external loads, ensuring robust dynamic performance. The fundamental design concept of SMC involves pre-designing a sliding surface on the phase plane and transitioning between different substructures via control input signals. SMC guides the system state variables towards the predesigned sliding surface and to enter the sliding mode. Once in sliding mode, the dynamic performance relies solely on the sliding surface and is immune to uncertainties in system parameters and external noise, thereby preserving the system's dynamic response.[18,19]

Owing to the nonlinear and discontinuous nature of sliding mode control as a high-speed switching feedback control method, the system's substructure swiftly switches to different quadrants in accordance with the control input signal, potentially leading to chattering phenomena in system dynamic responses. To address this, the design of adaptive SMCs within the framework of DTC has been studied.[20–22] These adaptive controllers are tailored to enhance the speed-tracking control performance and robustness in the face of varying system parameters and external disturbances. Indeed, designing an SMC becomes challenging when uncertainties and variation ranges in system parameters cannot be predetermined. Building upon the DTC architecture for motors, we present the design of an integrated controller that combines the flux SMC and the speed SMC, incorporating time delay estimation. This integrated controller is aimed at achieving closed-loop speed control of the PMSM, providing a more effective and robust control strategy. The proposed system demonstrates robustness, particularly in enhancing the speed control performance of PMSMs, even when faced with certainties in motor parameters and external loading.

2. Controller Design for PMSM

The mathematical equations of the PMSM can be summarized as follows.[1]

$$v_d = \left(r_s + L_d \frac{d}{dt} \right) i_d - \omega_r L_q i_q \tag{1}$$

$$v_q = \left(r_s + L_q \frac{d}{dt} \right) i_q + \omega_r L_d i_d + \omega_r \lambda'_m \tag{2}$$

$$T_e = \frac{3}{2}\frac{P}{2}\left[\lambda'_m i_q + \left(L_d - L_q \right) i_d i_q \right] \tag{3}$$

$$T_e = J \frac{d}{dt} \omega_m + B\omega_m + T_L \tag{4}$$

Here, v_d and i_d are the d-axis voltage and current, respectively; v_q and i_q stand for the q-axis voltage and current; ω_r and ω_m are the electrical angular speed of the rotor magnetic field and the rotor angular speed, respectively; λ'_m indicates the equivalent magnetic flux strength of the

permanent magnet; T_e is the electrical torque; P is the number of rotor magnetic pole; J is the moment of inertia of the motor and load; B is the friction coefficient; and T_L is the load torque. The electrical and mechanical angular velocity relationship can be expressed as $\omega_r=(2\omega_m)/P$. According to the flux-orientation control principle,[1,3] the stator magnetic flux λ_s overlaps the x-axis of the x-y axis reference coordinate, as shown in Fig. 1. Then, under the consideration of $L_d = L_q = L_s$, the dynamic equation can be rewritten as the following equations for the DTC method:[1,8]

$$\dot{\lambda}_s = -r_s i_x + v_x \tag{5}$$

$$\dot{\omega}_m + \left(\frac{B}{J} + \frac{k_T P \,|\, \lambda_s \,|}{2Jr_s} \right) \omega_m + \frac{T_L}{J} = \frac{k_T}{Jr_s} v_y \,, \tag{6}$$

where $k_T=(3P / 4)|\lambda_s|$; $\lambda_s = L_s i_x + \lambda'_m \cos\delta$ is the stator flux rotating at synchronous speed. x–y is the stator flux synchronous rotation reference coordinates, d–q is the rotor reference coordinates, and α–β is the static reference coordinates. The rotor magnetic flux λ_d is located on the d-axis. The angle $\delta = \theta_s - \theta_r$ represents the angle between the stator and rotor flux.

2.1 Stator flux SMC design

Equation (5) can be rearranged as follows:

$$\dot{\lambda}_s = -r_{sn} i_x + u_\lambda - d(t) \,, \tag{6}$$

where $u_\lambda = v_x$ and $d(t) = \Delta r_s i_x$; r_{sn} indicates the average resistance of each phase on the stator side, and Δr_s is its corresponding uncertainty value. Next, the flux tracking error can be defined as e_λ, where λ_{sd} and λ_s denote the constant flux command and resultant stator flux linkage, respectively. Then, the sliding function of stator flux in sliding mode control can be expressed as

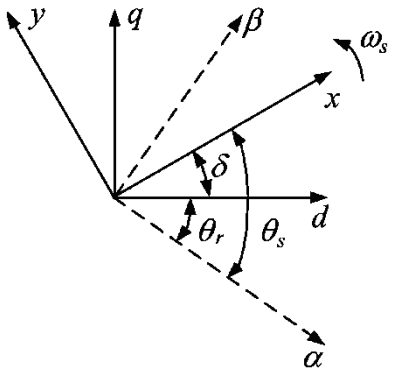

Fig. 1. Diagram for stator flux overlap x-axis.

$$s_\lambda(t) = e_\lambda(t) + \int_0^t k_\lambda e_\lambda(\tau) d\tau \,, \tag{7}$$

where $k_\lambda > 0$ is the design parameter, and the sliding surface is defined as $s_\lambda(t) = 0$. Then, the derivative of the sliding surface to time can be yielded as

$$\dot{s}_\lambda = k_\lambda e_\lambda + r_{sn} i_x - u_\lambda + d(t) = 0 \,. \tag{8}$$

The ideal control law can be obtained as Eq. (9), which is obtained by simply applying the cancellation method and embedding the desired dynamic to achieve $\dot{s}_\lambda = 0$.

$$u_{\lambda eq} = k_\lambda e_\lambda + r_{sn} i_x + d\left(t\right) \tag{9}$$

Given the uncertainty of system parameters, the stator flux SMC can be designed as

$$u_\lambda = \hat{u}_\lambda + \beta_\lambda sgn(s_\lambda) \,, \tag{10}$$

where $\hat{u}_\lambda = k_\lambda e_\lambda + r_{sn} i_x$ is the best approximation control input without uncertainty, β_λ is the switching gain of its controller, and $sgn(\cdot)$ is the sign function. Defining the Lyapunov function $V = s_\lambda^2 / 2$, the stability analysis of the stator flux SMC can be derived as

$$\begin{aligned} \dot{V}_\lambda &= s_\lambda \{k_\lambda e_\lambda + r_{sn} i_x - [k_\lambda e_\lambda + r_{sn} i_x + \beta_\lambda sgn(s_\lambda)] + d(t)\} \\ &= s_\lambda [d(t) - \beta_\lambda sgn(s_\lambda)] \\ &\le |d(t)||s_\lambda| - \beta_\lambda |s_\lambda| \\ &\le -\left[\beta_\lambda - |d(t)|\right]|s_\lambda| \le -\eta_\lambda |s_\lambda| \,, \end{aligned} \tag{11}$$

where $\eta_\lambda > 0$ is the design parameter and $\beta_\lambda \ge |d(t)| + \eta_\lambda$ is a sufficient condition to ensure the negative definite of $\dot{V}_\lambda$. This means that s_λ will be asymptotically converged to zero if V_λ is positive definite and $\dot{V}_\lambda$ is negative definite. Then, on the basis of Eq. (11) and the sliding surface condition of $\dot{s}_\lambda = 0$, the stator flux tracking error e_λ will also be asymptotically converged to zero along with the sliding surface when the time approaches infinity. In addition, to reduce the chattering phenomenon, the controller Eq. (10) can be redesigned as below by directly transferring the $sgn(\cdot)$ function into $sat(\cdot)$.[23]

$$u_\lambda = k_\lambda e_\lambda + r_{sn} i_x + \beta_\lambda sat\left(s_\lambda \Big/ \phi_\lambda \right) \tag{12}$$

Here, ϕ_λ is the boundary layer thickness, and it is the design parameter for reducing the effectiveness of the chattering phenomenon.

2.2 Speed SMC with time delay estimation

Equation (6) is rewritten as below as the proposed speed controller design for consistency in symbolic presentation.

$$\dot{\omega}_m = -a\omega_m - f + bu_\omega \tag{13}$$

$a = B/J + \left(k_T P|\lambda_s|/2Jr_s\right)$, $f = T_L/J$, $b = k_T/Jr_s$, and $u_\omega = v_y$. Considering the uncertainties of system parameters and loading torque (T_L), the above equation can be represented as below.

$$\dot{\omega}_m = \left[-a\omega_m - f + (b-\hat{b})u_\omega\right] + \hat{b}u_\omega = H_\omega(t) + \hat{b}u_\omega \tag{14}$$

Next, defining the speed tracking error as $e_\omega = \omega_{md} - \omega_m$, the sliding function of speed sliding mode control is expressed as

$$s_\omega(t) = e_\omega(t) + \int_0^t k_\omega e_\omega(\tau)d\tau\,, \tag{15}$$

where $k_\omega > 0$ is also the design parameter for speed control, and the corresponding sliding surface is defined as $s_\lambda(t) = 0$. Similarly, the derivative of the sliding surface to time can be presented as Eq. (16) when the condition on the sliding surface is guaranteed.

$$\dot{s}_\omega = \dot{e}_\omega + k_\omega e_\omega = \dot{\omega}_{md} - H_\omega(t) - \hat{b}u_\omega + k_\omega e_\omega = 0 \tag{16}$$

Using the simple techniques of canceling the undesired and embedding the desired dynamics, the ideal control law can be obtained to achieve $\dot{s}_\omega = 0$, which means "on the sliding surface".

$$u_{\omega eq} = \hat{b}^{-1}\left(\dot{\omega}_{md} - H_\omega(t) + k_\omega e_\omega\right) \tag{17}$$

When uncertainties arise owing to changes in system parameters and loading torque T_L, the unknown function $H_\omega(t)$ can be approximated by the function at a small time delay L[20] and expressed as

$$H_\omega(t) \approx H_\omega(t-L) = \dot{\omega}_{md}(t-L) - \hat{b}u_\omega(t-L)\,. \tag{18}$$

When the time delay L is small, the relationship between $H_\omega(t)$ and $H_\omega(t-L)$ can be expressed as

$$\left|H_\omega(t)-H_\omega(t-L)\right|\le r_\omega\,, \tag{19}$$

where $\gamma_\omega>0$. Then, the speed SMC with time delay estimation can be expressed as

$$u_\omega=\hat{u}_\omega+\hat{b}^{-1}k_2 sgn(s_\omega)\,, \tag{20}$$

where $\hat{u}_\omega$ is the best approximate control input, and k_2 is the controller switching gain. $\hat{u}_\omega$ can be expressed as

$$\hat{u}_\omega=u_\omega(t-L)+\hat{b}^{-1}\left[\dot{\omega}_{md}-\dot{\omega}_m(t-L)+k_\omega e_\omega\right]. \tag{21}$$

Furthermore, by defining the Lyapunov function $V_\omega=s_\omega^2/2$, the stability analysis of the speed SMC with time delay estimation can be derived as

$$\begin{aligned}\dot{V}_\omega&=\left[\dot{\omega}_{md}-H_\omega(t)-\hat{b}u_\omega+k_\omega e_\omega\right]\\&=\left[-H_\omega(t)+H_\omega(t-L)-k_2 sgn(s_\omega)\right]s_\omega\\&\le-\left[k_2-\left|H_\omega(t)-H_\omega(t-L)\right|\right]\left|s_\omega\right|\le-\eta_\omega\left|s_\omega\right|,\end{aligned} \tag{22}$$

where $\eta_\omega>0$ is the design parameter and k_2 is also a design parameter that must satisfy the following condition.

$$k_2\ge\gamma_\omega+\eta_\omega \tag{23}$$

When $\dot{V}_\omega(e_\omega,t)$ is negative definite and $V_\omega(e_\omega,t)$ is positive definite, the speed control system is asymptotically stable. This indicates that s_ω will gradually converge to zero when t approaches infinity ($t\to\infty$). When the sliding mode occurs on the sliding surface of Eq. (16), it represents $s_\omega=\dot{s}_\omega=0$. Suppose k is chosen as a positive number. In that case, the speed error will gradually slide to the origin along with the sliding surface because it is asymptotically stable. In addition, to reduce the chattering phenomenon caused by the controller, the speed controller can be directly modified by the following Eq. (24), according to Ref. 23.

$$u_\omega=u_\omega(t-L)+\hat{b}^{-1}\left[\dot{\omega}_{md}-\dot{\omega}_m(t-L)+k_\omega e_\omega+k_2 sat(s_\omega/\phi_\omega)\right] \tag{24}$$

Here, φ_ω is the boundary layer thickness, and it is the design parameter for reducing the effect of the chattering phenomenon. Figure 2 illustrates a robust sliding mode DTC system of PMSM.

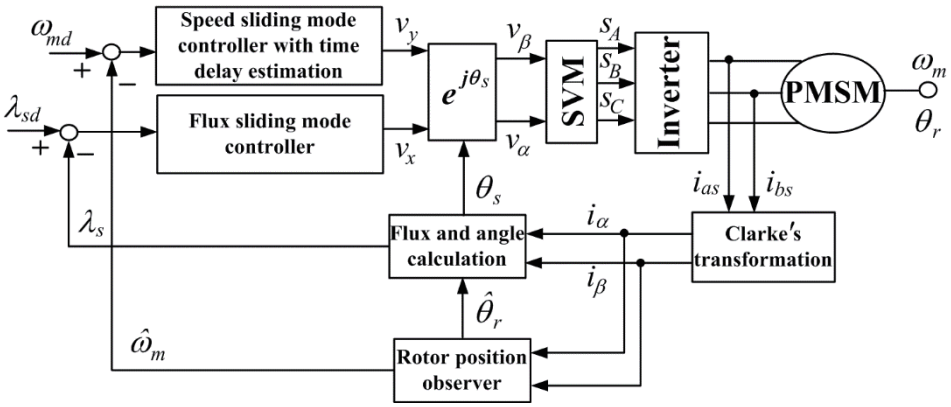

Fig. 2. Diagram for robust sliding mode DTC system of PMSM.

3. Simulation Results and Discussion

In this paper, we focused on the surface-mounted PMSM as the studied motor, and the relevant parameters are outlined in Table 1. In the simulation control system presented in this paper, an SVM with a carrier frequency of 20 kHz is employed, and the stator magnetic flux command value is set to 0.1 Wb. The parameters for the speed SMC with time-delay estimation are configured, where L is set to the sampling period (1/20 kHz). For effective motor speed control and stable convergence of the speed tracking error (e_ω), the proportional gain (k_ω) must exceed 0. To meet this criterion, choosing k_ω as 2.5 ensures a well-performing dynamic response of the speed control system. The stator flux SMC, requiring a response speed significantly faster than the speed SMC, sets k_λ to 10 in accordance with the design condition of $k_\lambda > (4 \sim 8) k_\omega$. Additionally, referring to the results of the stability analysis of the Lyapunov functions in Eqs. (11) and (22), the parameters are designed as follows: η_λ = 30, η_ω = 20, and $\phi_\lambda = \phi_\omega$ = 0.1. Moreover, considering variations in system parameters Δr_s, Δa, and Δf, a range of 20% around the nominal values is adopted.

Figure 3 depicts the outcomes of robust sliding mode speed control with time-delay estimation, named the time-delay SMC method. The motor achieves the speed control target within 0.12 s during the acceleration phase, displaying a smooth and stable speed response. In Fig. 3(b), noticeable speed errors are observed at 0.02 and 0.12 s when the speed command follows a ramp curve. These errors stem from the inherent sudden acceleration changes during the initiation and attainment of the speed set by ramp commands. However, the speed tracking performance remains commendable for other ramp speed commands. In Figs. 3(c) and 3(d), we examine the input voltage and current responses designed by the stator flux SMC; introducing 20% stator resistance uncertainty leads to significant chattering phenomena in the control input response. Figures 3(e) and 3(f) illustrate the y-axis input and current response outcomes of the robust sliding mode speed control with time-delay estimation, revealing a noticeable reduction in control input chattering phenomena. Introducing a curved speed command improves speed

Table 1
PMSM parameters.

Paramter	Surface-mounted PMSM
Rated speed	3000 rpm
Stator resistance (r_{vs})	2.875 Ω
Direct axis inductor (L_d)	8.5×10^{-3} H
Quadrature axis inductor (L_q)	8.5×10^{-3} H
Equivalent magnetic flux of permanent magnet (λ'_m)	0.175 Wb
Mechanical moment of inertia (J)	0.8×10^{-3} kg·m^2
Mechanical viscous friction coefficient (B)	0 Nm/(rad/s)
Number of poles (P)	8

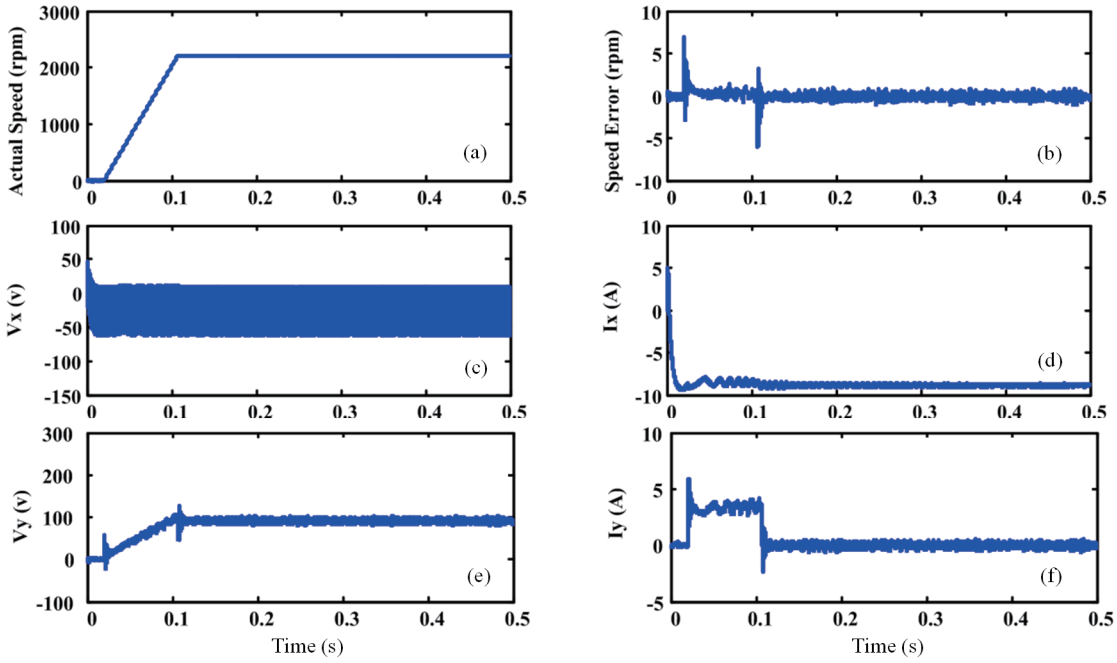

Fig. 3. (Color online) Result of robust sliding mode speed control with time-delay estimation for forward rotation of 2200 rpm under the condition of no load. (a) Actual speed response. (b) Speed error response. (c) x-axis voltage input. (d) x-axis current response. (e) y-axis voltage input. (f) y-axis current response.

tracking errors during startup and the transition to a constant speed. Additionally, excellent speed tracking performance is maintained under curved speed commands. As demonstrated in Figs. 4(a) and 4(b), the steady-state speed errors have been kept within 1 rpm.

Figure 5 illustrates the simulated responses of a PMSM under a ramp speed command ω_{md} of 2200 rpm and an instantaneous load torque variation T_L at $t = 0.3$ s. It is essential to emphasize that we have systematically compared four types of speed control method: proportional-integral vector control (PIC), proportional-integral DTC (PI+DTC), SMC, and time-delay SMC. In Fig. 5(a), the PMSM demonstrates a rise time of 0.12 s, displaying a smooth and stable overall speed curve across all control strategies. Compared with PI+DTC, PIC exhibits a significant overshoot, reaching the steady-state speed at approximately 0.165 s. In Fig. 5(b), when instantaneous load

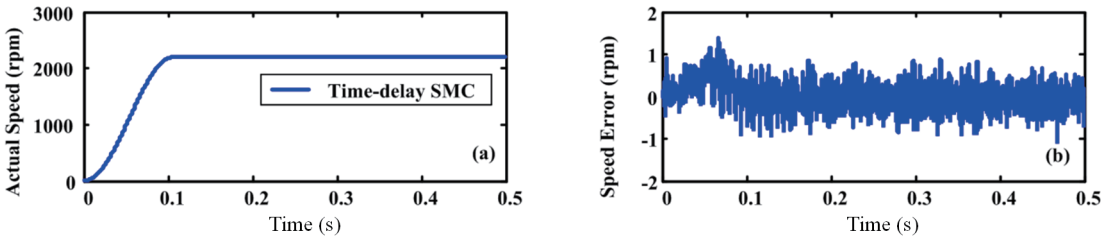

Fig. 4. (Color online) Result of robust sliding mode speed control with time-delay estimation for forward rotation of 2200 rpm and s-curve under the condition of no load. (a) Actual speed response. (b) Speed error response.

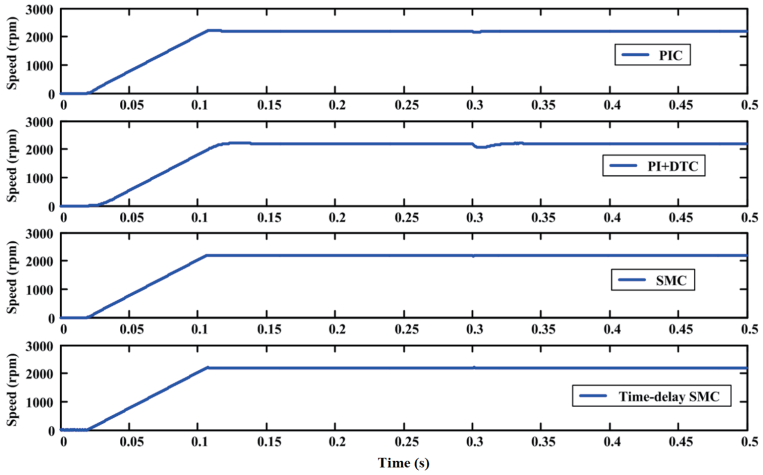

(a)

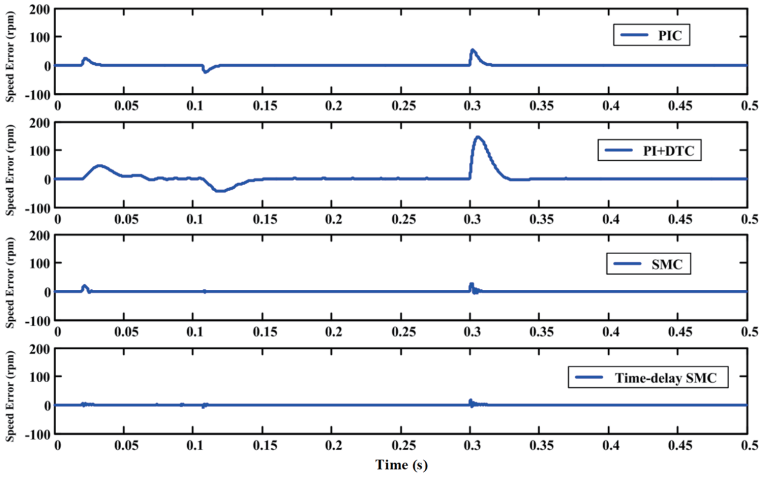

(b)

Fig. 5. (Color online) Speed control response of 2200 rpm: (a) rotational speed, (b) rotational speed tracking error, and (c) torque response.

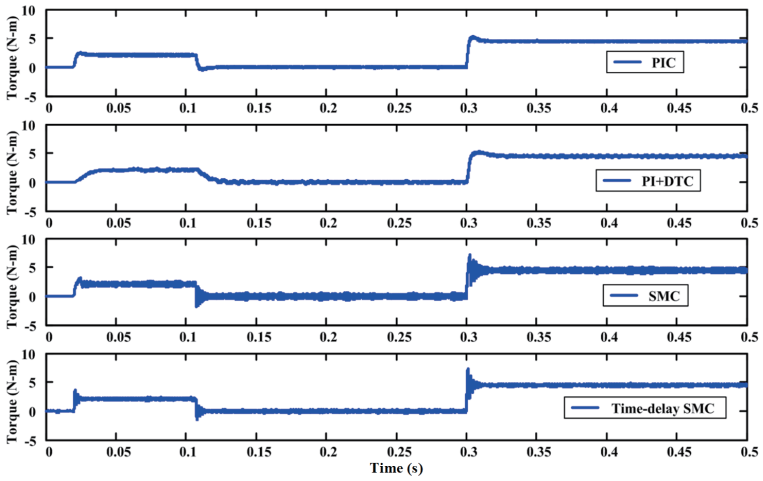

(c)

Fig. 5. (Color online) (continued) Speed control response of 2200 rpm: (a) rotational speed, (b) rotational speed tracking error, and (c) torque response.

T_L changes to 130% of the rated torque (increased to 4 N·m) at t = 0.3 s, a comparison of the four control strategies reveals distinctive behaviors. PIC experiences a speed drop of approximately 40 rpm, taking 0.03 s to recover to the designed speed control performance. PI+DTC exhibits a speed drop of about 60 rpm, taking 0.06 s to return to the designed speed tracking performance. Concerning instantaneous load variations, SMC and time-delay SMC exhibit 20 and 10 rpm speed drops, respectively, and recover to the designed speed tracking performance within 0.02 s. Time-delay SMC proves to be superior when comparing the torque ripples of the above two SMC methods.

Figure 6 depicts the responses of a PMSM under a ramp speed command ω_{md} set to 100 rpm in a positive rotation, accompanied by an instantaneous load torque variation T_L of 50% of the rated torque and a doubling of the mechanical rotational inertia J at t = 0.3 s. Notably, Figs. 6(a) and 6(b) highlight the significant impact on the speed results of PI+DTC. However, SMC and time-delay SMC display speed drops of 5 and 1.5 rpm, respectively. These two methods can recover to the designated speed control target within 0.02 s. The results in Figs. 6(b) and 6(c) underscore the excellent robust control of time-delay SMC in the face of parameter variations and instantaneous load changes. Time-delay SMC exhibits a rapid response and minimal speed tracking errors in low-speed control compared with the other three controllers.

Figure 7 shows that the speed control response of a PMSM is evident under a ramp speed command of ω_{md} = 100 rpm, with the stator resistance r_s varying to twice the rated value. The results in Fig. 7(b) highlight periodic variations in the speed error control outcomes of PI+DTC. Specifically, Figs. 7(b) and 7(c) reveal that when the motor operates at low speed and the stator voltage is minimal, variations in stator resistance lead to inaccurate stator flux estimation, consequently diminishing the speed control performance of the system. However, the speed errors are consistently maintained within a specific range for SMC and time-delay SMC. Time-delay SMC is the optimal choice as it achieves consistent control results with very small speed errors.

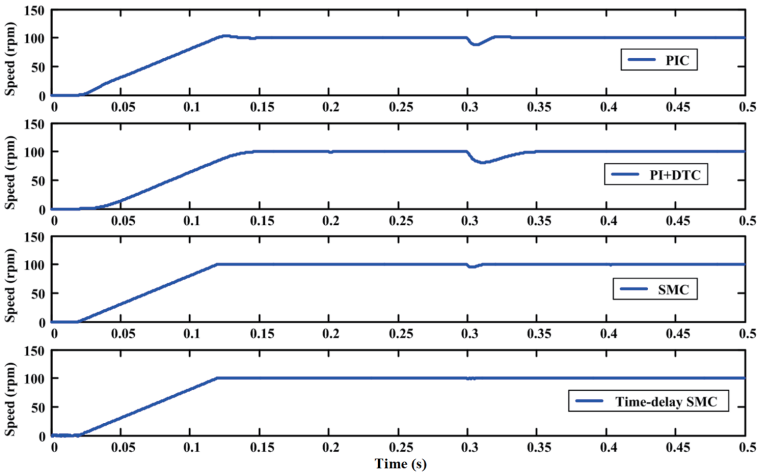

(a)

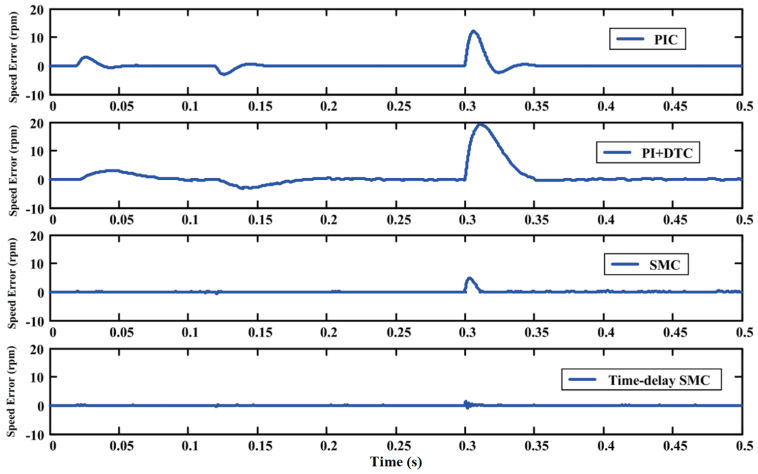

(b)

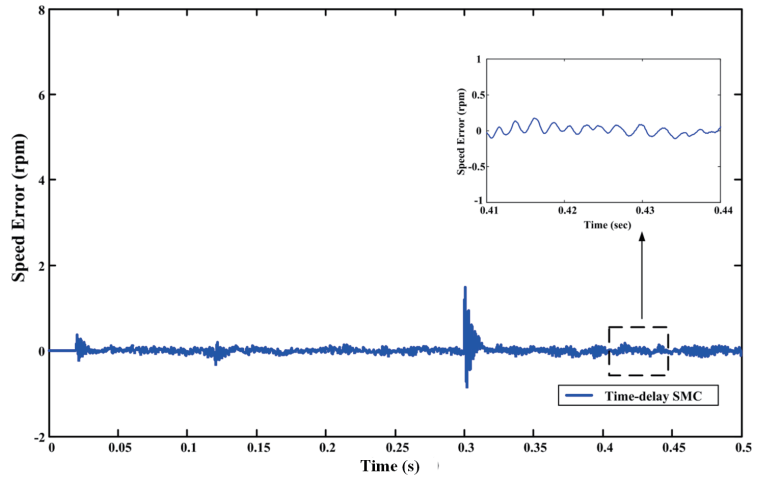

(c)

Fig. 6. (Color online) Response of PMSM with ramp speed command of 100 rpm in forward direction under uncertainties of J variation and instant loading (T_L) variation at t = 0.3 s. (a) Rotational speed response, (b) rotational speed tracking response, and (c) regional amplification of speed error for sliding mode speed control with time delay estimation.

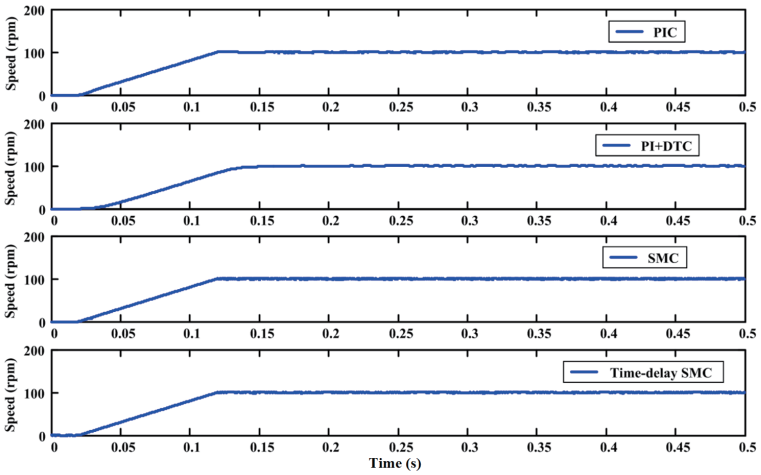

(a)

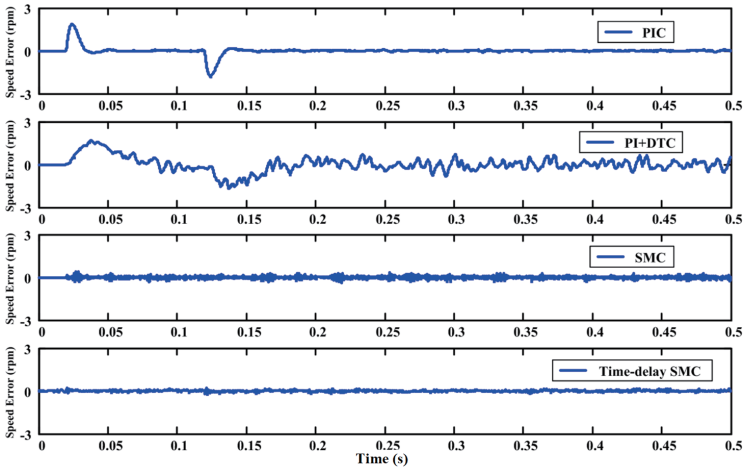

(b)

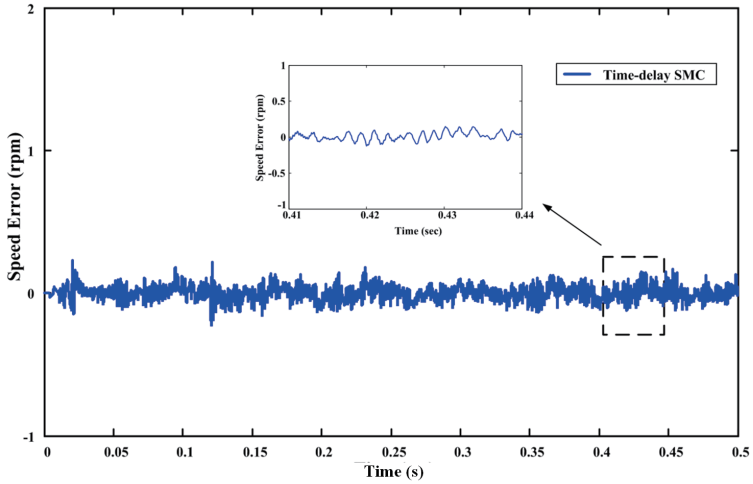

(c)

Fig. 7. (Color online) Response of PMSM with ramp speed command of 100 rpm in forward direction under uncertainties of stator resistance (r_s) variation. (a) Rotational speed response, (b) rotational speed tracking response, and (c) regional amplification of speed error for sliding mode speed control with time delay estimation.

4. Conclusions

We introduced a novel controller design employing a time-delay SMC for the speed control of a PMSM within a DTC system architecture. In the study, we comprehensively compared a PI controller and the proposed SMC, evaluating their performance under forward rotation and diverse trajectory tracking scenarios. As presented in this paper, the time-delay SMC shows exceptional dynamic responses for speed, stator flux, and electromagnetic torque across both high- and low-speed command conditions. Notably, with uncertain system parameters and instantaneous external loads applied to the PMSM, the time-delay SMC exhibits superior command input tracking and robust characteristics. It outperforms both PIC and PI+DTC in achieving more stable speed dynamic responses. To further validate its performance, future work should involve the practical implementation of the proposed controller in real controlled systems, leveraging a DSP core. Such implementation would offer valuable insights into the controller's effectiveness in practical applications.

Acknowledgments

This research was partially supported by projects under grant No. CS-111-03.

References

1 S. J. Chapman: Electric Machinery Fundamentals, McGraw-Hill Education International (New York, 2015) 5th ed., Chap. 3.
2 D. W. J. Pulle, P. Darnell, and A. Veltman: Applied Control of Electrical Drives, Springer International Publishing (Switzerland, 2015) Chap. 2.
3 F. Mendoza-Mondragón, V. M. Hernández-Guzmán, and J. Rodríguez-Reséndiz: IEEE Trans. Ind. Electron. **65** (2018) 6099. https://doi.org/10.1109/TIE.2017.2786203
4 R. Ghassani, Z. Kader, M. Fadel, P. Combes, and M. Koteich: Proc. 2023 IEEE Int. Electric Machines & Drives Conf. (IEEE, 2023) 1–7. https://doi.org/10.1109/IEMDC55163.2023.10239079
5 J. C. Nustes, D. P. Pau, and G. Gruosso: Software Impacts **15** (2023) 100479. https://doi.org/10.1016/j.simpa.2023.100479
6 C. Zhang, X. Wang, D. Wang, Q. Sun, and G. Ma: Proc. 2019 22nd Int. Conf. Electrical Machines and Systems (IEEE, 2019) 1–4. https://doi.org/10.1109/ICEMS.2019.8921693
7 F. Niu, B. Wang, A. S. Babel, K. Li, and E. G. Strangas: IEEE Trans. Power Electron. **31** (2016) 1408. https://doi.org/10.1109/TPEL.2015.2421321
8 D. Casadei, F. Profumo, G. Serra, and A. Tani: IEEE Trans. Power Electron. **17** (2002) 779. https://doi.org/10.1109/TPEL.2002.802183
9 A. A. H. Khamis, A. M. A. Abbas, and M. A. M. Algoul: Proc. 2022 IEEE 2nd Int. Maghreb Meeting of the Conf. Sciences and Techniques of Automatic Control and Computer Engineering (IEEE, 2022) 75–80. https://doi.org/10.1109/MI-STA54861.2022.9837649
10 V. Fireteanu and A.-I. Constantin: Proc. 2022 Int. Symp. Power Electronics, Electrical Drives, Automation and Motion (IEEE, 2022) 246–251. https://doi.org/10.1109/SPEEDAM53979.2022.9842230
11 S. S. Kale and R. C. Pawaskar: Proc. 2018 Int. Conf. Advances in Communication and Computing Technology (IEEE, 2018) 45–49. https://doi.org/10.1109/ICACCT.2018.8529651
12 L. A. Mohammed: Proc. 2019 2nd Int. Conf. Electrical, Communication, Computer, Power and Control Engineering (IEEE, 2019) 148–152. https://doi.org/10.1109/ICECCPCE46549.2019.203764
13 J.-D. Zhang, F. Peng, Y.-K. Huang, Y. Yao, and Z.-C. Zhu: Proc. 2020 Int Conf. Electrical Machines (IEEE, 2020) 2358–2364. https://doi.org/10.1109/ICEM49940.2020.9270806
14 X. Wang, Z. Wang, Z. Xu, M. Cheng, and Y. Hu: IEEE Trans. Ind. Electron. **67** (2020) 10095. https://doi.org/10.1109/TIE.2019.2962451

15 N. Taghizadegan, M. B. B. Sharifian, A. Daghigh, and E. Babaei: Proc. 2011 Int. Conf. Electrical Machines and Systems (IEEE, 2011) 1–5. https://doi.org/10.1109/ICEMS.2011.6073466
16 X. Zhou, H. Zhao, and J. Zhu: Proc. 2015 Int. Conf. Intelligent Informatics and Biomedical Sciences (IEEE, 2015) 385–389. https://doi.org/10.1109/ICIIBMS.2015.7439509
17 K. H. Ang, G. Chong, and Y. Li: IEEE Trans. Control Syst. Technol. **13** (2005) 559. https://doi.org/10.1109/TCST.2005.847331
18 C. Edwards and S. K. Spurgeon: Sliding Mode Control Theory and Applications, Taylor & Francis Inc. (Pennsylvania, 1998) Chaps. 3 and 4.
19 S. E. Ryvkin and E. P. Lever: CRC Press (London, 2012) 1st ed., Chaps. 2 and 4.
20 T. Li, Y. Zhao, and L. Hou: IEEE Access **11** (2023) 17021. https://doi.org/10.1109/ACCESS.2023.3245635
21 Q. Wang, H. Yu, M. Wang, and X. Qi: IEEE Access **7** (2019) 36691. https://doi.org/10.1109/ACCESS.2019.2903439
22 B. Tang, W. Lu, B. Yan, K. Lu, J. Feng, and L. Guo: IEEE Trans. Ind. Electron. **69** (2022) 12621. https://doi.org/10.1109/TIE.2021.3137587
23 J.-J. Slotine and W. Li: Applied Nonlinear Control, Prentice Hall (New Jersey, 2019) Chap. 7.